ASTRONOMY AND ASTROPHYSICS

HST images and properties of the most distant radio galaxies

L. Pentericci[1], H.J.A. Röttgering[1], G.K. Miley[1], P. McCarthy[2], H. Spinrad[3], W.J.M. van Breugel[4], and F. Macchetto[5]

[1] Leiden Observatory, P.O. Box 9513, 2300 RA Leiden, The Netherlands
[2] The Observatories of the Carnegie Institution of Washington, 813 Santa Barbara Street, Pasadena, CA 91101, USA
[3] Astronomy Department, University of California, Berkeley, CA 94720, USA
[4] Lawrence Livermore Laboratory, P.O. Box 808, Livermore, CA 94459, USA
[5] Space Telescope Science Institute, 3700 San Martin Drive, Baltimore, MD 21218, USA

Received 8 July 1998 / Accepted 16 October 1998

Abstract. With the Hubble Space Telescope we have obtained images of 9 of the most distant radio galaxies. The galaxies, which have redshifts between $z = 2.3$ and $z = 3.6$, were observed with the WFPC2 camera in a broad band filter (F606W or F707W, roughly equivalent to V or R-band), corresponding to the near ultraviolet emission in the rest frame of the radio galaxies. The total observing time was 2 orbits per object. In this paper we present the images overlayed on VLA radio maps of comparable resolution. We also present previously unpublished images, taken from the HST archive, of two other high redshift radio galaxies, observed through similar broad band filters. We find that on the scale of the HST observations there is a wide variety of morphological structures of the hosting galaxies: most objects have a clumpy, irregular appearance, consisting of a bright nucleus and a number of smaller components, suggestive of merging systems. Some observed structures could be due (at least partly) to the presence of dust distributed through the galaxies. The UV continuum emission is generally elongated and aligned with the axis of the radio sources, however the characteristics of the "alignment effect" differ from case to case, suggesting that the phenomenon cannot be explained by a single physical mechanism. We compare the properties of our radio galaxies with those of the UV dropout galaxies and conclude that (i) the most massive radio galaxies may well evolve from an aggregate of UV dropout galaxies and (ii) high redshift radio galaxies probably evolve into present day brightest cluster galaxies.

Key words: galaxies: individual: TX 1707+1051 – galaxies: individual: MRC 2104+242 – galaxies: formation – galaxies: clusters: general – galaxies: active – cosmology: early Universe

1. Introduction

Studying the optical morphology of high redshift ($z > 2$) radio galaxies (HZRGs) can contribute substantially to our understanding of galaxy formation and evolution in the early universe (for a recent review see McCarthy 1993). Although the recent development of new techniques (e.g. U and B band dropouts, Steidel et al. 1996) has led to the discovery of a large population of high redshift galaxies, radio galaxies remain still of exceptional interest, because they pinpoint the most massive systems at high redshift and are potential signposts for finding high-redshift clusters of galaxies.

It has been shown that high luminosity radio sources associated with quasars and radio galaxies at redshift ~ 0.5 are located in rich clusters (e.g. Hill & Lilly 1991). At $z \sim 1$ there are now several possible X-ray clusters that have been discovered around powerful radio galaxies, such as 3C324 at z=1.2 (Dickinson et al. 1998), 3C356 and 3C280 (Crawford & Fabian 1996). At $z > 2$ the existence of clusters around HZRGs has not been established. However, there is an increasing number of important observational indications that HZRGs might be in clusters, including (i) the detection of possibly extended X-ray emission from the radio galaxy PKS 1138-262 at z=2.156, most probably coming from a hot cluster atmosphere (Carilli et al. 1998); (ii) strong Faraday polarization and rotation of the radio emission of some HZRGs which might be due to dense gaseous halos (Carilli et al. 1997); (iii) possible excess of companion galaxies detected along the axes of the radio sources (Röttgering et al. 1996); (iv) possible excess of Lyman break selected galaxies in the fields of several powerful radio sources (e.g. Lacy & Rawlings, 1996) and (v) excess of candidate companion galaxies (with two objects spectroscopically confirmed) in the vicinity of MRC 0316-257, at z=3.14 (Le Fevre et al. 1996).

The hosts of powerful low redshift radio sources have long been identified with giant elliptical galaxies, containing old stellar population. The surprising continuity of the K–z relation between the high redshift radio galaxies and the low redshift brightest cluster galaxies which shows little scatter up to redshift of ~ 4 (although the scatter increases beyond redshift 2, e.g. Eales et al. 1997), might indicate that the hosts of powerful radio sources are the most massive galaxies know at high–redshifts. Moreover, since HZRGs are probably located in forming clusters of galaxies, they could be the ancestors of brightest cluster galaxies.

We have previously presented and discussed HST images of the radio galaxy PKS 1138-262 at z=2.156, which shows the

Send offprint requests to: L. Pentericci (laurastrw.leidenuniv.nl)

clumpiest optical morphology of all the HZRGs imaged with the HST (Pentericci et al. 1998). Our conclusion was that PKS 1138-262 is giant elliptical galaxy at the center of a protocluster in the late stages of its formation.

In this paper we present HST–WFPC2 images for 9 powerful radio galaxies having redshifts between z=2.3 and z=3.6. We also present deep HST archive images of 2 HZRGs observed with WFPC2. We compare the HST images with VLA maps of the associated radio sources having similar resolution. After discussing the sample selection (Sect. 2), we describe the HST imaging and reduction procedures (Sect. 3), the radio imaging and the problem of the relative astrometry between the radio and HST data (Sect. 4). In Sect. 5 we briefly discuss the most important characteristics of each object, also referring to previous results that are relevant to the interpretation of the new data. Finally in Sect. 6 we discuss some statistical trends of the properties of these high redshift radio sources, giving a qualitative interpretation. We then summarize our main results and present our conclusions. We also include the Appendix new radio images of the radio galaxies TX 1707+105 and MRC 2104-242.

Throughout this paper we assume a Hubble constant of $H_0 = 50\,\mathrm{km\,s^{-1}\,Mpc^{-1}}$ and a deceleration parameter of $q_0 = 0.5$.

2. Sample selection

The radio galaxies were initially selected from the more than 60 HZRGs which were known at the commencement of the project (1995) (e.g. van Ojik 1995 and references therein). Most of these distant radio galaxies were found by observing ultra steep spectrum radio sources (USS) ($\alpha < -1.0$, where α is the radio spectral index) (van Ojik 1995).

Objects were selected according to the following criteria: (i) bright in the the R band (R$<$ 24, i.e. sufficient to be mappable in a reasonable time with the HST); (ii) amongst the brightest line emitters (Lyα flux $> 10^{-15}\,\mathrm{erg\,s^{-1}cm^{-2}}$). Because of its high redshift, we also included the radio galaxy MG 2141+192 (z=3.594) in the sample.

Finally we obtained unpublished HST/WFPC2 images of the radio sources B2 0902+343, at z=3.395, and TX 0828+192, at z=2.572, from the HST archive.

For a statistical study of the properties of HZRGs it is important to enlarge the sample of objects with HST images: we therefore included in our analysis the other radio galaxies that have been imaged with the HST. These include the radio galaxy 4C 41.17 at z=3.8, one of the the best studied HZRGs (van Breugel et al. 1998); the radio galaxy PKS 1138-262, at z=2.156 that was studied by our group (Pentericci et al. 1997, 1998); MRC 0406-242 at z=2.44 that was object of a multi-frequency study, including WFPC imaging in different color bands, by Rush et al. (1997); and 4C 23.58 at z=2.95 (Chambers et al. 1996a and 1996b). The first two objects were imaged with the WFPC2 camera, while the last two were imaged with the pre-refurbishment HST/WFPC. Details of the observations can be found in the mentioned papers. In this way the final sample available for the statistical analysis of the properties of HZRGs consists of 15 galaxies. By including also radio galaxies that have been imaged with the pre-refurbishment HST and/or for which the total integration times are considerably different (e.g. the observations of 4C 41.17 are much deeper than for the other objects), the quality of the images varies within the sample. However given the relatively small number of radio galaxies observed, it is important to increase the statistics.

In addition to the HST images, all the radio galaxies in the final sample have been imaged with the VLA at several frequencies, to study their radio-polarimetric properties (Carilli et al. 1997) and have Lyα profiles taken with resolution of $< 100\,\mathrm{km\,s^{-1}}$, thus allowing a detailed study of the morphology and kinematics of the ionized gas (van Ojik et al. 1997). For some of the radio galaxies, ground-based narrow band images of the Lyα emission gas, and broad band images in various color bands (mostly R-band and K-band) are also available (see references for individual objects in Sect. 5).

3. HST imaging

3.1. Observations

Table 1 summarizes the observations. 9 radio galaxies were imaged with the Planetary Camera (PC) of WFPC2 during Cycle 5 and/or Cycle 6. The PC utilizes an 800 $\times$ 800 pixel Loral CCD as detector with pixel size of $0.0455''$ (Burrows 1995). The typical exposure time was 5300 sec (2 orbits) for each galaxy. The total observing time was split between two exposures to facilitate removal of cosmic ray events.

The filters used for the observations were chosen to avoid contamination from the strong Lyα emission line at 1216 Å and to have the rest frame wavelengths sampled as similar as possible throughout the sample. For the radio galaxies at redshift $z > 2.9$ the filter used was the broad-band F707W filter (centered at $\lambda_0 = 6868\,$Å and with a FWHM of $\Delta\lambda = 1382\,$Å), similar to the Cousins R band; for the lower redshift galaxies we used the broad-band F606W filter ($\lambda_0 = 5934\,$Å and $\Delta\lambda = 1498\,$Å) which is similar to the V band.

The radio galaxy TX 0828+193 was observed during Cycle 4 with the WFPC2 by Chambers et al., using the filter F675W which is centered at $\lambda_0 = 6756\,$Å and has a FWHM of $\Delta\lambda = 865\,$Å. The observations were done in polarimetric mode. The galaxy was observed using the WF3 section of WFPC2, which utilizes an 800 $\times$ 800 pixel Loral CCD as detector with pixel size of $0.1''$ (Burrows 1995). The total exposure time of 10000 s was split between ten observations.

The radio galaxy B2 0902+343 was observed during Cycle 4 by Eisenhardt and Dickinson, using the PC of WFPC2 with the filter F622W, which is centered at $\lambda_0 = 6189.9\,$Å and has a FWHM of $\Delta\lambda = 916\,$Å. The total exposure time of 21600 s was split between nine observations.

In the redshift range observed the continuum emission may include contribution from the faint emission lines of HeII, CIII] and CIV. For most of the radio galaxies we could estimate the total contamination using the line fluxes measured by low resolution spectra of the objects taken by van Ojik (1995) . The detected lines are listed in Table 1, as well as the total contribution of the line emission to the measured flux, which ranges from

Table 1. Observation log

Cat.	Source	z	Obs. date	Filter	Rest.$\lambda\lambda$ Å	Exp. time sec.	N	WFPC mag	Lines	%flux[a]
(1)	(2)	(3)	(4)	(5)	(6)	(7)	(8)	(9)	(10)	(11)
TX	0211−122	2.336	14/8/95	F606W	1554-2003	5300	2	22.9	HeII,CIII]	13.7
TX	1707+105	2.349	7/8/95	F606W	1550-1998	5300	2	23.7[b]	HeII,CIII]	4.2[c]
4C	1410−001	2.363	15/8/95	F606W	1542-1987	5300	2	22.9	HeII,CIII]	13.3
MRC	2104−242	2.491	10/5/97	F606W	1485-1914	5300	2	22.5	–	–
TX	0828+193	2.572	26/1/96	F675W	1770-2012	10000	10	22.2	CIII]	5.1
MRC	2025−218	2.630	9/11/95	F606W	1428-1841	5300	2	22.6	–	–
4C	1345+245	2.879	29/3/97	F702W	1592-1949	5200	2	23.4	none	≤ 1
MRC	0943−242	2.923	18/11/95	F702W	1575-1927	5300	2	22.6	HeII,CIII]	11.0
B2	0902+343	3.395	5/11/94	F622W	1304-1512	21600	9	23.8	–	–
4C	1243+036	3.570	5/8/95	F702W	1352-1654	5300	2	23.2	none	≤ 1
MG	2141+192	3.594	10/5/97	F702W	1345-1645	5200	2	24.2	–	–

(1) Catalog. (2) Source name. (3) Redshift. (4) Date of HST observations. (5) Filter used for HST observations. (6) Rest-frame wavelength interval in angstroms. (7) Total exposure time in second. (8) Number of frames in which the total observing time was split. (9) WFPC2 magnitude within an aperture of radius $4''$. (10) Emission line detected within the filter band. (11) Percentual flux contamination from the detected lines.

[a] See text for a detailed explanation

[b] Magnitude of galaxy 1707+105A

[c] Contribution to the total flux of 1707+105A and 1707+105B.

0 to 13.7%, with the highest contribution for the radio galaxy TX 0211-122. We expect that for the 4 sources of which we do not have any such data available, the line contribution will be in the same range. Therefore we can assume that the images represent to a good approximation the continuum emission from the galaxies.

3.2. Data Processing

The data were reduced according to the standard Space Telescope Science Institute pipeline (Lauer 1989). Further processing was performed using the NOAO Image Reduction and Analysis Facility (IRAF) software package and the Space Telescope Science Data Analysis System (STSDAS) and involved cosmic ray removal and registering of the images. The shifts were measured from the peak positions of a non-saturated star present in both the PC images. The different frames were then added, background subtraction was performed using the average flux contained within 4 or more apertures placed on blank areas of the sky, as close as possible to the source, at different positions, to avoid introducing errors from residual gradients in the background flux. The resulting image was flux calibrated according to the precepts described in the "HST Data Handbook" (1995 edition), using the photometric parameters from the standard HST calibration and included in the file header. The images were then rotated to superimpose them to the VLA radio maps (see Sect. 4.1)

The magnitudes were computed from the unrotated images (which have less smoothing) within a fixed aperture of diameter $4''$. In most cases this aperture is large enough to enclose all the light from the galaxies. The magnitudes were computed as: $m = -2.5log_{10}F + M(0)$, where F is the measured flux and $M(0) = 21.1$ is the zero point for the HST magnitude scale normalized to Vega. The results are presented in Table 1.

A number of different effects contributes to the errors in the photometric magnitudes; (i) the Poisson noise of the detected counts; (ii) a $\sim$2% uncertainty in the determination of the zero point (Burrows 1995); (iii) a $\sim$4% systematic error due to the problem of charge transfer efficiency in the Loral CCD (Holtzman et al. 1995) for which we did not correct; (iv) accurate subtraction of the mean sky background; (v) sky noise within the source aperture. The last two are usually the predominant effects. We estimate that the total uncertainty in the magnitudes is 0.1 or less for all galaxies.

A first order transformation from the F606W and F702W ST magnitudes to the standard magnitude system was derived applying the precepts described by Holtzman et al. (1995). The resulting transformation are $m_V = m_{F602W} + 0.25(V - I)$, $m_R = m_{F622} - 0.25(V - R)$, $m_V = m_{F675W} + 0.21(V - R)$,and $m_R = m_{F702} + 0.3(V - R)$.

In Table 1 we list for each galaxy the WFPC magnitude m; the emission lines that have been detected within the filter band and the total line contribution to the continuum flux.

4. Radio imaging

All the radio galaxies with the exception of B2 0902+343, TX 1707+105 and MRC 2104-242 were imaged with the VLA as part of a high resolution, multi-frequency radio polarimetric study carried out on a large sample of HZRGs by Carilli et al.

Table 2. Properties of the radio sources

Source	RA J2000	Dec J2000	$F_{4.5}$ mJy	α	$CF_{4.5}$ %	Size kpc	RM rad m^{-2}	PA	Ref.
(1)	(2)	(3)	(4)	(5)	(6)	(7)	(8)	(9)	(10)
TX 0211−122	02:14:17.37	−11:58:46.7	54	1.5	3.8	134	160	73[a]	A
TX 1707+105	17:10:06.85	+10:31:09.0	64	1.2	–	173	–	-58	C
4C 1410−001	14:13:15.13	−00:22:59.6	57	1.3	6.7	189	1510	44[a]	A
MRC 2104−242	21:06:58.16	−24:05:11.3	68	1.3	1.6	177	–	12	B
TX 0828+193	08:30:53.71	+19:13:18.5	22	1.6	21	98	–	-42	A
MRC 2025−218	20:27:59.45	−21:40:57.1	95	1.1	0.7	38	910	-16	A
4C 1345+245	13:48:14.78	+24:15:50.0	115	1.4	0.7	17	750	-36	A
MRC 0943−242	09:45:32.79	−24:28:49.8	55	1.8	–	29	–	75	A
B2 0902+343	09:05:30.10	+34:07:56.9	100	1.4	15	32	2500	37	E
4C 1243+036	12:45:38.43	+03:23:20.3	70	1.4	2.0	50	420	20	D
MG 2141+192	21:44:07.50	+19:29:15.0	67	1.6	–	60	–	3	A

(1) Name of the source (2) and (3) coordinates of the radio core in the epoch J2000. (4) Total radio flux at 4.5 GHz. (5) Radio spectral index between 4.5 GHz and 8.2 GHz, $S_\nu = S_0\nu^{-\alpha}$. (6) Radio core flux /total flux at 4.5 GHz rest-frame. (7) Maximum radio source size. (8) Maximum rotation measure. (9) Position angle of the inner radio axis relative to the direction North-South. (10)
References: A: Carilli et al. 1997, B: McCarthy et al. 1990, C: This paper, D: van Ojik et al. 1996, E: Carilli 1995
[a] Radio jets might be precessing.

(1997). A full description of the observations and the reduction procedure can be found in this paper.

The radio map of B2 0902+343 that we use in this paper is a high resolution (0.15″) radio continuum image of total intensity at 1.65GHz obtained by Carilli by combining data from the VLA and MERLIN (see Carilli 1995 for details).

The radio observations of TX 1707+105 and MRC 2104−214 were performed with the VLA in B array. Details of observations and reduction for both sources can be found in Appendix A and B.

4.1. Relative astrometry

The coordinate frame for the WFPC2 images determined from the image header information has uncertainties of the order of $1''$ (Burrows 1995). Since the optical galaxies are generally clumpy on a scale smaller than $1''$, it is important to get the better possible registration between the radio and the optical images, to allow a detailed inter-comparison between the emissions.

In overlaying the HST images with the radio VLA images we made the following assumptions: for those sources showing a clear detection of the radio nucleus and for which good K-band (or K_{sh}-band) images existed (McCarthy, private communication), we assumed that the peak position of the infra-red image would be a better indicator of the true location of the center of the host galaxy than the peak of the HST image, since the UV continuum might be affected by dust extinction (e.g de Koff et al. 1996). We therefore identified the position of the radio core in the VLA image with the peak position of the K-band image. Finally we registered the HST frame and the infrared frame using the weighted positions of several stars which were present on both fields; this can be achieved with an accuracy of $0.1''$ which is then the total final uncertainty in the relative astrometry. This procedure was possible for the radio galaxies TX 0211-122, 4C 1243+036, MRC 2025−218 and MRC 2104−242.

For those objects which had a clearly detected radio core but no K-band images, we associated the peak position of the HST image to the peak position of the radio emission. We followed this procedure for the radio galaxies 4C 1345+245, 4C 1410-001 and TX 0828+128 (for this last object see remarks made in the individual source description): these objects have a relatively simple morphology, hence it is reasonable to assume that the peak of the UV continuum represents the true nucleus of the galaxy; the final uncertainty of the relative astrometry is then within a pixel i.e. $\sim 0.05''$.

For those objects which have no detected radio core (MRC 0943−242, TX 1707+105 and MG 2141+192) we used the HST absolute astrometry, and we then checked the peak position of several stars which were present on the WFPC2 frames, with the position given in the APM catalog; with this method we achieved an accuracy of $\sim 0.8''$. Finally for B2 0902+343 which has a radio core but no clear optical nucleus, we kept the natural HST astrometry: in this way the radio core falls in between the two optical peaks. This is consistent with what was found e.g. by Carilli (1995).

5. Individual source description

Grey scale HST WFPC2 images (smoothed with a Gaussian function of FWHM equal to 2 pixels) with VLA radio contours superimposed are shown in Figs. 1–10. For every source we also show a contour map of the continuum emission to better delineate the morphology. We do not show such maps for B2 0902+343 and MG 2141+192 because they have very low surface brightness, and a contour map would add no information. For the very large radio galaxies (namely TX 0211-122, TX 1707+105 and 4C 1410-001) we also present a third image

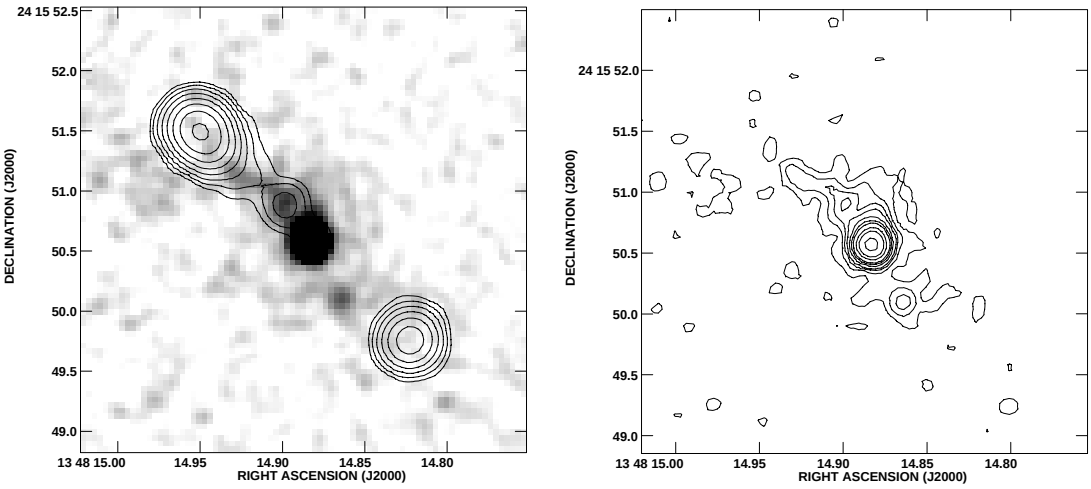

Fig. 1. *Left*: A grey scale continuum image of 4C 1345+245 at $z = 2.879$ with VLA radio contours superimposed. Radio contours are a geometrical progression in 2, with the first contour at 0.2mJy, which is 3 times the rms background noise. *Right*: Contour representation of the UV continuum emission. Contours are at 11,12,13,14,16,20,25,30,40 $\times 4.910^{-22}$ erg s^{-1} Å^{-1}.

showing the complete field of the radio source. The objects are presented in order of increasing radio size, since it has been shown (e.g van Ojik 1995) that several properties of HZRGs tend to change with increasing radio size.

We shall now give brief descriptions of the ultraviolet morphology of each radio galaxy, with special emphasis on any peculiar characteristics (such as distortions, jet-like features etc), and compare those with relevant previous results.

4C 1345+245

This radio source at z=2.879 (Chambers et al. 1996a), is the smallest in the sample, being only $2''$ in extent (corresponding to 17 kpc in the adopted cosmology). The radio structure has been extensively studied with the VLA at several frequencies by Carilli et al. (1997), who classified it as "compact steep spectrum source" (CSS) and by Chambers et al. (1996b). The radio emission shows two lobes of roughly equivalent brightness, with a one sided feature extending from the core towards the eastern side, which has been identified as a jet. Optical and infrared ground–based observations show a compact object, with the emission extended along the radio axis, with one faint component or companion object along the radio axis to the southwest but beyond the radio lobe. (Chambers et al. 1996a). The new HST image shows that in UV continuum the emission has a bright compact nucleus. On the eastern side of this component there is a jet-like feature that follows remarkably well the small curvature of the radio jet: this suggests that we might be observing the optical counterpart of the radio-jet. However the radio-to-optical spectral index derived from the flux of the component (0.7) is completely different from the high-frequency radio spectral index (-1.2). Such flattening of spectral indices into the optical is contrary to what is found for sources with observed optical synchrotron radiation (e.g. Meisenheimer et al. 1989). Therefore we discard this possibility. A more likely interpretation is that star formation is taking place in that region triggered by the passage of the radio jet. Other possible mechanisms to enhance the emission along the radio jet path have been proposed by Bremer et al. (1997). In Sect. 6.1 we will discuss more extensively the alignment effect and how all the various models that have been proposed to explain it, apply to our sample of radio galaxies.

The object along the radio axis detected by Chambers et al. (see above) is also detected in our HST image (it is outside the field shown in Fig. 1); its morphology indicates that it is most probably an edge-on spiral (hence a foreground object).

MRC 0943-242

This radio source at z=2.923 (Röttgering et al. 1995) is only 29 kpc in extent and has a simple double-morphology, with no nucleus detected in the present VLA images (Carilli et al. 1997). The HST image shows a bright elongated main component, plus a number of smaller clumps embedded in a halo of lower surface brightness emission with a peculiar overall curved morphology. The inner region of the UV emission shows a remarkably good alignment (within 10°) with the radio axis. For comparison,the Keck K-band image taken by van Breugel et al. (1998) shows a somewhat rounder and more centrally concentrated morphology.

High resolution spectroscopy of the Lyα line shows spatially resolved absorption by associated neutral hydrogen, with the absorber covering the entire extended Lyα emission (Röttgering et al. 1995). Similar deep high resolution observations have been performed on the CIV and HeII lines: the HeII line does not show absorption, which is expected as this is a resonant line, while the CIV line shows absorption due to the CIV 1548/1551 doublet. The column density for the absorber is $10^{14.4}$ cm^{-2}. Combined with the measured column density for the HI absorber, this indicates that the spatially extended absorber is metal enriched (Röttgering & Miley 1996).

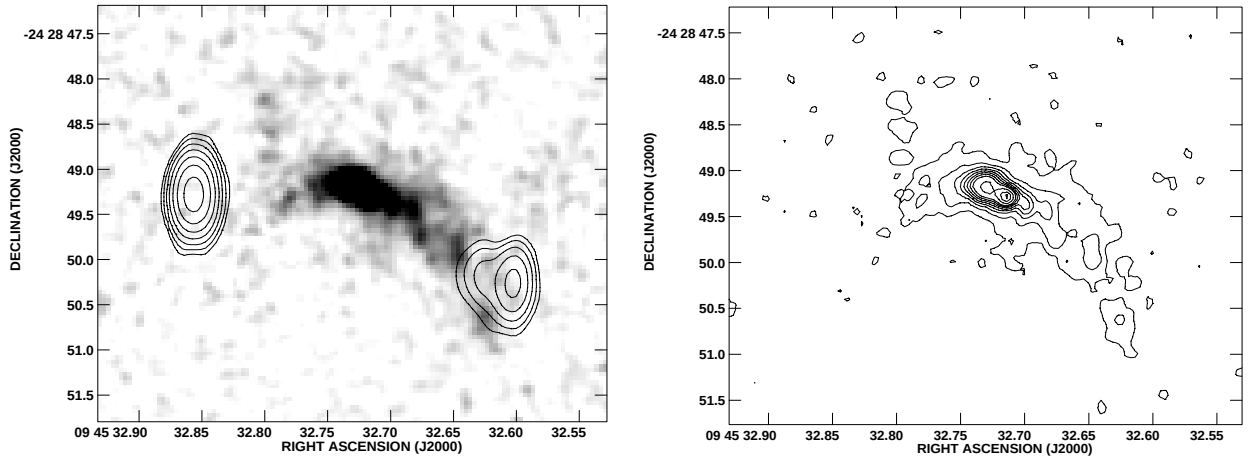

Fig. 2. *Left*: Grey scale image of MRC 0943−242 at z=2.923, with VLA radio contours superimposed. Contours are a geometrical sequence in steps of 2 with the first contour at 0.15 mJy which is 3 times the background noise. *Right*: Contour representation of the UV continuum emission. Contour levels are: 5,6,7,8,9,10,11,12,14,16,18,20 $\times 1.2510^{-21}$ erg s^{-1} Å^{-1}.

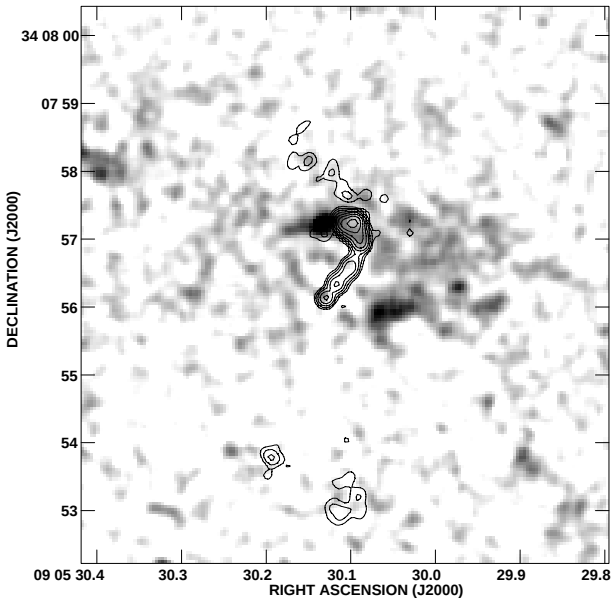

Fig. 3. Grey scale representation of the continuum emission from B2 0902+343 z=3.395, with VLA contours superimposed. Contours are at geometrical sequence in steps of 2 with the first contour at 0.5 mJy.

B2 0902+343

This radio galaxy was identified by Lilly (1988) and is one of the most extensively studied high redshift radio galaxies. It is 32 kpc in extent.

The radio emission has a bizarre structure showing a bright knotty jet with a sharp bend of almost 90° at its northern end, and two southern components whose common orientation is perpendicular to the rest of the source (Carilli et al. 1994). Further multi-frequency radio studies lead Carilli (1995) to conclude that most of the peculiarities of the radio galaxy can be explained by assuming that the source is oriented at a substantial angle (between 45 and 60 degrees) with respect to the plane of the sky, with the northern regions of the source approaching and that the central region of the galaxy is obscured by a substantial amount of dust.

From extensive studies Eisenhardt & Dickinson (1992) found that B2 0902+343 has a flat optical spectral energy distribution (SED), and an unusually low surface brightness distribution at optical and IR wavelengths; this lead to the suggestion that B2 0902+343 might be a proto-galaxy, undergoing a first major burst of star formation (Eales et al. 1993, Eisenhardt & Dickinson 1992). The presence of associated 21 cm neutral hydrogen in absorption against the radio continuum source was first detected by by Uson et al. (1991) and confirmed by others (Briggs et al. 1993, de Bruyn 1996). However no strong absorption in the Lyα emission line has been detected (Martin-Mirones et al. 1995).

The optical morphology, as imaged by the HST, confirms the unusually low surface brightness distribution and shows that the galaxy consists of 2 regions, of approximately the same flux with a void in between, plus an extended fuzzy emission region to the north east of them. The source does not exhibit the radio-optical alignment effect; the UV emission is almost perpendicular to the radio axis. With the present astrometry the radio core is situated in a valley between the optical peaks; this morphology could be explained with the presence of large amounts of dusts. However the uncertainties in the astrometry are such that the radio core could be coincident with any of the two optical components.

MRC 2025-218

The galaxy associated with this USS radio source at z=2.630 (38 kpc in extent), was first identified by McCarthy et al. (1990). Deep multi-frequency radio imaging show a double radio source with a jet on the southern side of the core, which has an extremely sharp bend towards the west, making an angle of $\sim 90^\circ$ (Carilli et al. 1997). The northern lobe has a faint extension in the direction of the core which could be a counter–jet. Ground–based near infrared imaging show a compact object (van Breugel et al. 1998), while the Lyα emission extends for more than

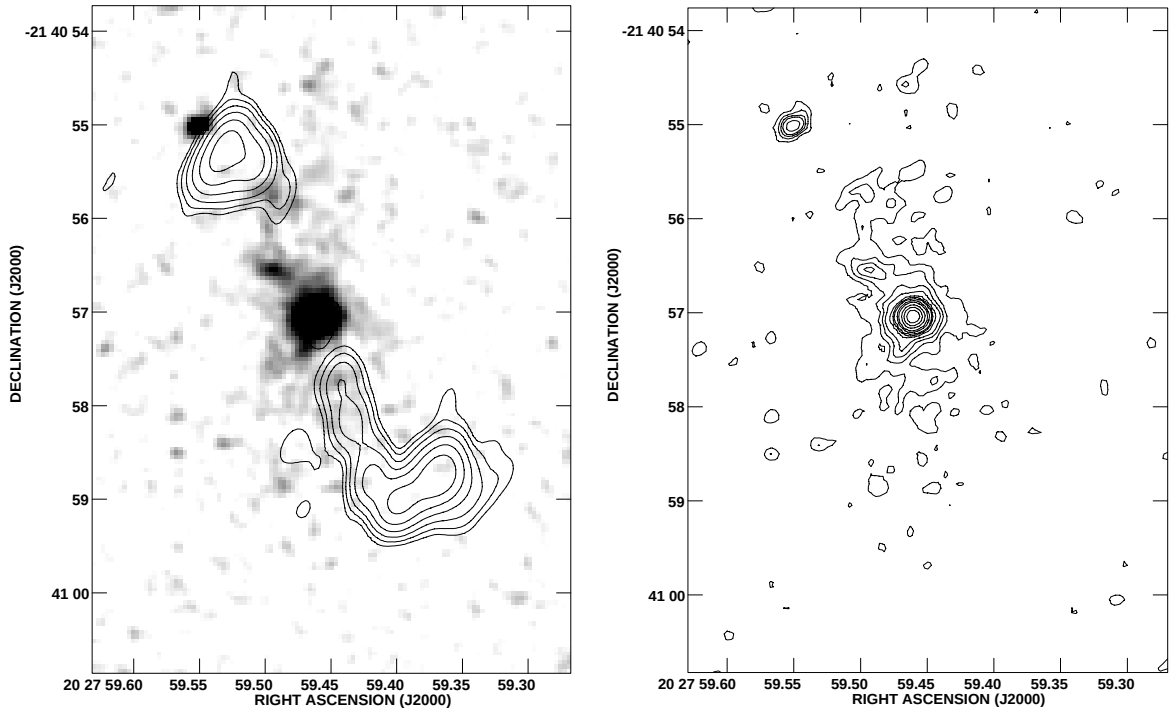

Fig. 4. *Left*: Grey scale image of MRC 2025−218 at z=2.630, with VLA radio contours superimposed. Contours are a geometrical sequence in steps of 2 with the first contour at 0.15 mJy. *Right*: Contour representation of the UV continuum emission. Contour levels: 5,6,7,8,9,10,11,12,14,16,18,20 $\times 1.2510^{-21}$ erg s^{-1} Å^{-1}.

5″ along the radio axis and is distributed bimodally. The total SED of the galaxy is well fit by a main stellar population aged 1.5 Gyrs, combined with a young star-burst contributing 20% of the total light at 5000 Å (McCarthy et al. 1992). Cimatti et al. (1993) find that the rest frame UV continuum emission is linearly polarized ($P = 8.3 \pm 2.3\%$), with the electric vector oriented perpendicular to the UV emission axis.

The HST image shows that the host galaxy has a compact morphology, consisting of a bright nucleus, two smaller components and extended low surface brightness emission, which is elongated and well aligned with the radio axis. The angle between the inner radio axis and the extended UV emission is only $\sim 5^\circ \pm 3^\circ$. There is no direct one-to-one relation between the radio components and the UV emission, unlike 4C 1345+245; however if we draw a cone of opening angle $\sim 30^\circ$ along the radio axis, all the UV emission on both sides of the radio core is then constrained within this cone. Such a morphology, reminiscent of an ionization cone, is expected in models where the aligned UV continuum emission is scattered light of a buried quasar, and is supported by the polarization measurements by Cimatti et al. (1993).

The present HST image reveals little UV emission near the bend: however high resolution spectroscopic observations of the Lyα emission line show that the galaxy is embedded in a very large halo of ionized gas, extended well beyond the radio source (more than 60 kpc i.e. double the size of the radio source); therefore the most likely explanation for the bend is that interaction between the radio plasma and the surrounding gas deflects the jet, as observed in other cases (e.g. Pentericci et al. 1997).

4C 1243+036

This radio galaxy at z=3.570 which has an extension of 50 kpc, was identified and extensively studied by van Ojik et al. (1996). The radio source is double with a sharp bent structure on the southern side. Strong depolarization of the radio emission indicates that the source is embedded in a magneto-ionic medium. High resolution spectroscopy and narrow band imaging of the Lyα emission line have detected the presence of a giant (100 kpc) halo of ionized gas showing ordered motion, possibly due to rotation of a proto-galactic gas disk, out of which the galaxy associated with 4C 1243+036 is forming. Furthermore the Lyα emission shows a secondary peak at the location of the bending of the radio jet, consistent with a gas cloud being responsible for the deflection of the radio jet (Ojik et al. 1996).

The morphology of the galaxy as imaged by the HST consists of a nucleus from where a narrow and elongated structure departs, which then bends to the south. There is also a smaller component, about 1″ beyond the northern radio hot spot, which could belong to the system, since narrow–band Lyα imaging shows that there is Lyα emission at this location (van Ojik et al. 1996).

The most remarkable characteristic of 4C 1243+036 is that the UV light follows closely the direction of the radio source, both in the inner 2″ region where the light is aligned with the radio axis to within 15 degrees, but especially at the location of the bend: here both the UV emission and the radio jet bend rather sharply to the south, suggesting a direct relation between the radio jet and the UV component. This is similar to the case

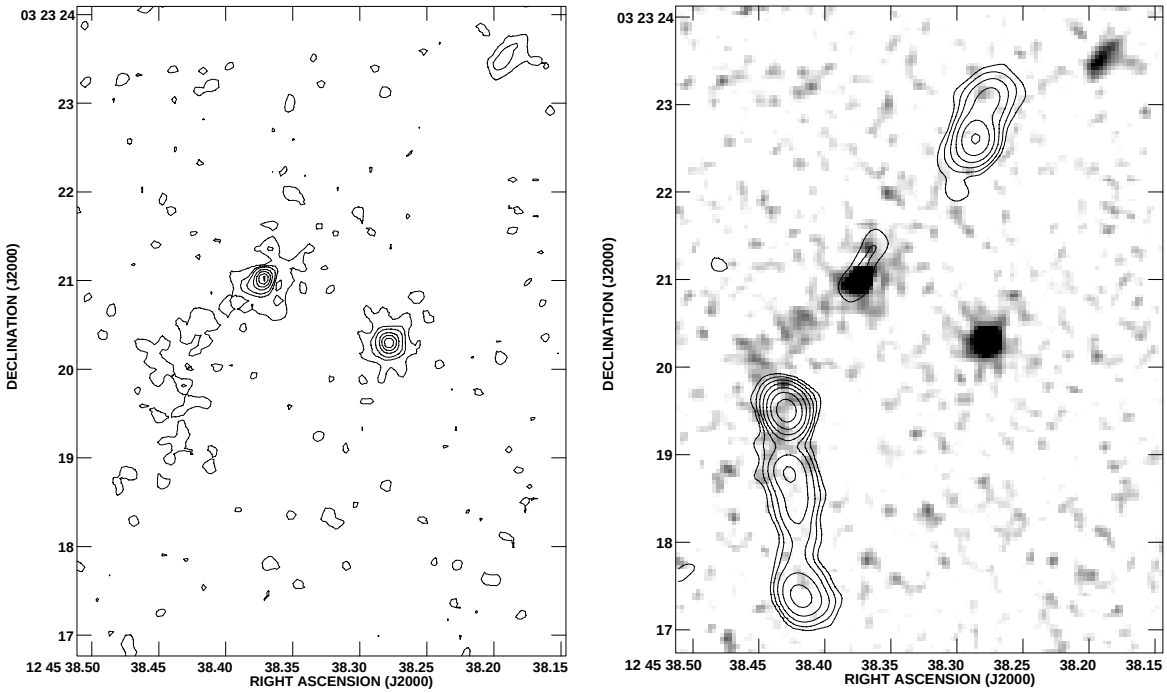

Fig. 5. *Left*: Grey scale image of 4C 1243+036 at z=3.570, with VLA contours superimposed. Contours are a geometrical sequence in steps of 2 with the first contour at 0.1 mJy. *Right*: Contour representation of the UV continuum emission. Contour levels:20,22,24,26,28,30 $\times 910^{-22}$ erg s^{-1} Å^{-1}.

of the radio galaxy 4C 1345+245. Note that recent K-band Keck imaging of 4C 1243+036 by van Breugel et al. (1998), although at a different resolution, indicate that also the K-band continuum emission is elongated and follows the bend of the radio jet.

MG 2141+192

This galaxy at z=3.594 (60 kpc in extent) was identified by Spinrad et al. (1992) and since then has been extensively studied by various groups. The radio source has a simple double morphology, with no nucleus detected in the present images. Eales & Rawlings (1996) who imaged this object in the infrared, report the detection of a relatively brighter component half way between the radio hot spots and a second fainter one, $4''$ north, approximately coincident with the northern radio hot spot. Recently van Breugel et al. (1998) re-imaged the object in the near-infrared with the Keck telescope, finding additional extended low surface brightness emission south of the nucleus. Armus et al. (1998) imaged the [OIII] emission line nebula associated with the galaxy, which has an extent of more than 70 kpc (equal to the separation between the radio lobes), is extremely narrow and aligned with the radio axis. By comparing fluxes of the different emission lines they also find indications for the presence of large amounts of dust. Finally Maxfield et al. (1997) find that the emission nebulae of Lyα, CIV and HeII are not only spatially extended but also have remarkable velocity structure with multi-components velocity displacement up to 1900 Km s^{-1}, which are most consistent with a shock ionization picture.

The HST shows that the host galaxy is very faint in the UV restframe, and consists of a nucleus with a faint filamentary extension and a small clump to the west. In the HST image some fuzzy emission (at a 3σ level) is present near the position of the radio hot spot, where the second infrared component is located. We also detect similar emission very close to the position of the southern radio component. Overall the UV rest-frame emission is extremely faint, consistent with the presence of large amounts of dust. Deeper images are needed to delineate the morphology of this galaxy in more detail.

TX 0828+193

This large radio source (98 kpc in extent) at z=2.572 (van Ojik 1995), has a double morphology with a jet extending from the core towards the northern hot spot (most probably the approaching side). The end of the jet contains multiple hot spots and has a 90 degrees bend. The southern part of the radio source consists only of a single hot spot.

The HST image shows a small galaxy consisting of several clumps arranged in a triangular shape. We choose to identify the radio core with the brightest optical component (the same procedure we followed for other galaxies, see Sect. 4); however another possible registration would be with the radio core at the vertex of the triangulum. At this position, an ionization cone on both sides of the radio core, would encompass all the UV emission. The morphology of TX 0828+193, like that of MRC 2025−218, strongly suggest that a large fraction of the UV light might be scattered light from a buried AGN. The axis of this

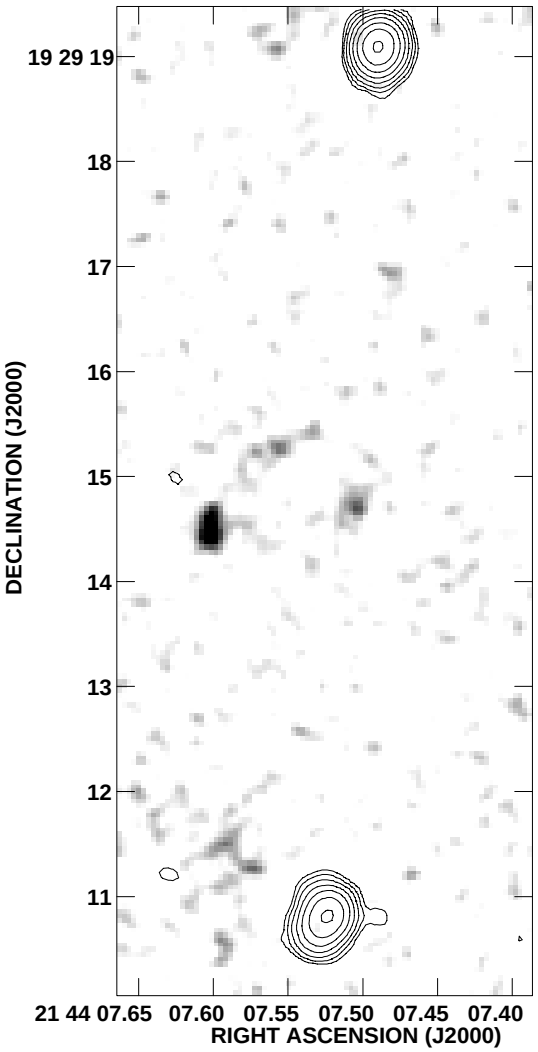

Fig. 6. Grey scale representation of the continuum emission of MG 2141+192 at z=3.594, with VLA radio contours superimposed. Contours are a geometrical sequence in steps of 2 with the first contour at 0.1 mJy.

"scattering cone" is aligned with the radio axis to within a few degrees ($7^\circ \pm 3^\circ$).

There is another object located along the radio axis which could be associated with the radio source (a companion galaxy): it is bright in the UV continuum but shows no line emission, so it could as well be an intervening system at a different redshift (van Ojik et al. 1997).

The Lyα emission from this radio galaxy has a spectacular shape, with the entire blue wing of the emission line profile absorbed by neutral gas associated with the galaxy (van Ojik et al. 1997). If the companion object is at the same redshift as TX 0828+193, then it is possible that a neutral gaseous halo associated with it is the responsible for the absorption. Since the absorption is very steep and broad, it is probably due to a combination of absorbing systems each at a slightly different velocity with respect to the Lyα peak. Also in the red wing of the Lyα profile a broad shoulder is observed that maybe be due to multiple HI absorption systems or to intrinsic velocity structure in the ionized gas.

TX 0211-122

This large radio source (134 kpc) at z=2.336 (van Ojik et al., 1994) has a simple double morphology. A jet feature extends from the core towards south, curves and reaches the eastern lobe; this structure suggests that the radio axis might be precessing.

The galaxy, as shown from the HST image, consists of a bright nucleus and a much smaller clump, both embedded by lower surface brightness emission, distributed in an irregular way. The contour image of the central component shows that it consists of two "tails", one of which points in the direction of the inner radio jet.

The optical spectrum of this source is peculiar with the Lyα emission being anomalously weak when compared to higher ionization lines: the flux ratio of Lyα to NV a factor of 30 smaller than that of typical HZRGs while the large NV/CIV ratio indicates that the line-emitting gas is over-abundant in nitrogen (van Ojik et al. 1994). Van Ojik et al. consider various mechanism that could produce these features, and conclude that the galaxy is likely to be undergoing a massive star-burst in the central region, possibly as the result of the passage of the radio jet. The star-burst would produce large amounts of dust, which when mixed through the emission line gas partly absorbs the Lyα emission, giving it a very patchy morphology, while the enhancement of nitrogen emission could be produced either by shocks or photo-ionization.

TX 1707+105

This radio source at z=2.349 (van Ojik 1995) which is 173 kpc in extent is one of the most peculiar systems in our sample: it consists of two galaxies (labeled A and B in Fig. 9) both showing strong and extended Lyα emission at the same redshift. The 2 objects lie almost exactly along the radio axis and they are both clumpy and elongated in a direction with is almost perpendicular to it. In particular galaxy 1707A (the brightest one) is comprised of a series of knots of approximately the same brightness, which form a sort of string, while galaxy 1707B consists of only two clumps. There is a further emission component, which in Fig. 9 is indicated as C, that lies in between the two galaxies and could be part of the system. It does not show line emission, although probably when the high resolution spectrum was taken this object fell outside our $2''$ wide slit.

With the present data it is not possible to determine exactly which galaxy is associated with the radio emission. Given the large extension of the source, we expect, for symmetry reasons, that the radio source is associated to the galaxy closest to the center, i.e. galaxy 1707A. If this is the case then 1707B, and possibly 1707C, would be companion galaxies located along the radio axis. There are many cases of companion galaxies of high and low redshift radio galaxies. The best known case is Minkowsky's object: the location of this dwarf galaxy is at the end of the radio jet emanating from the radio galaxy PKS

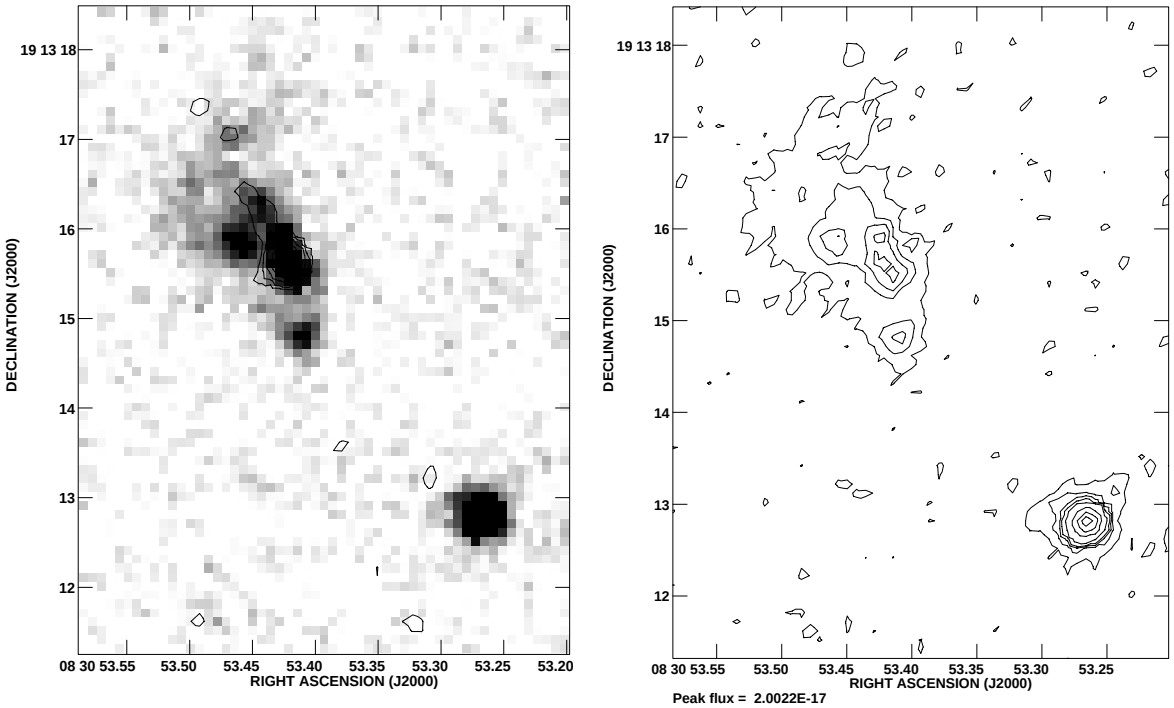

Fig. 7. *Left* Grey scale image of TX 0828+193 at z=2.572, with VLA contours superimposed. Contours are a geometrical sequence in steps of 2 with the first contour at 0.11mJy. *Right*: Contour representation of the UV continuum emission. Contour levels: 10,12,14,16,18,20,40,80 $\times 4.510^{-21}$ erg s^{-1} Å^{-1}.

0123−016 at $z = 0.0181$, suggesting that its origin is due to jet-induced star formation (van Breugel et al. 1985). A similar star forming region associated with the nearby powerful radio galaxy 3C285 has also been reported (van Breugel & Dey 1993). The most recent example is the radio source 3C34 (at z=0.69), which shows a clumpy emission feature along the radio axis and and oriented towards a radio hot spot. Also in this case, the emission has been associated with a region of massive star formation triggered by the passage of the radio jet (Best et al. 1997). Finally, Röttgering et al. (1996) find that companion galaxies of radio sources tend to be distributed along the direction of the radio axis, which, in their interpretation, could be due to the luminosity of merging dwarf galaxies being enhanced by scattering and/or jet-induced star formation.

MRC 2104-242

This radio galaxy at z=2.491 is 177 kpc in extent and was first identified by McCarthy et al. (1990). It has a simple double morphology and a relatively bright nucleus.

The Lyα emission is spectacular: narrow band imaging show two large gas clumps, extending for more than 12″ along the radio axis. Spectroscopy of the line showed that both components have very large velocity distribution (∼1000-1500 km s^{-1}), large equivalent width and have a net velocity difference of about 500 km s^{-1}. Each component contains multiple velocity peaks and kinematic data at various position angles indicate that there is no overall ordered motion (McCarthy et al. 1990, Koekemoer et al. 1996). A detailed study of the Lyα emission line showed that a model based on shocks from direct interaction between the radio plasma and the gas can explain both the kinematics and the morphology of the gas (Koekemoer et al. 1996).

The HST image is remarkable: the host galaxy is one of the clumpiest of our sample, consisting of a number of knots of similar brightness and size, located around the radio core. Unfortunately some of the components are confused with the residuals from a spike of an extremely bright nearby star. Furthermore there is a filamentary component that is more than 2″ long and extremely narrow. This last component is aligned with the radio axis to within a few degrees. The overall extension of the host galaxy is almost 7″, making it the largest optical galaxy in our sample.

4C 1410-001

This radio galaxy at z=2.363 (van Ojik, 1995) is, with 189 kpc, the largest radio source in the sample. The host galaxy is highly elongated ($\simeq 5''$). It consists of a compact nucleus, a second bright component and extended lower surface brightness emission which is clumpy. The galaxy and the radio source are strongly misaligned: the angle between the optical and radio axis is nearly 45 degrees. However, the northern component of the radio source is curved, suggesting the radio axis might be precessing, in which case the elongated optical emission could be located along the previous path of the radio jet. The galaxy has extended (~ 80 kpc) bright Lyα emission, exhibiting a velocity shear that could be due to rotation of the gas. The amplitude of

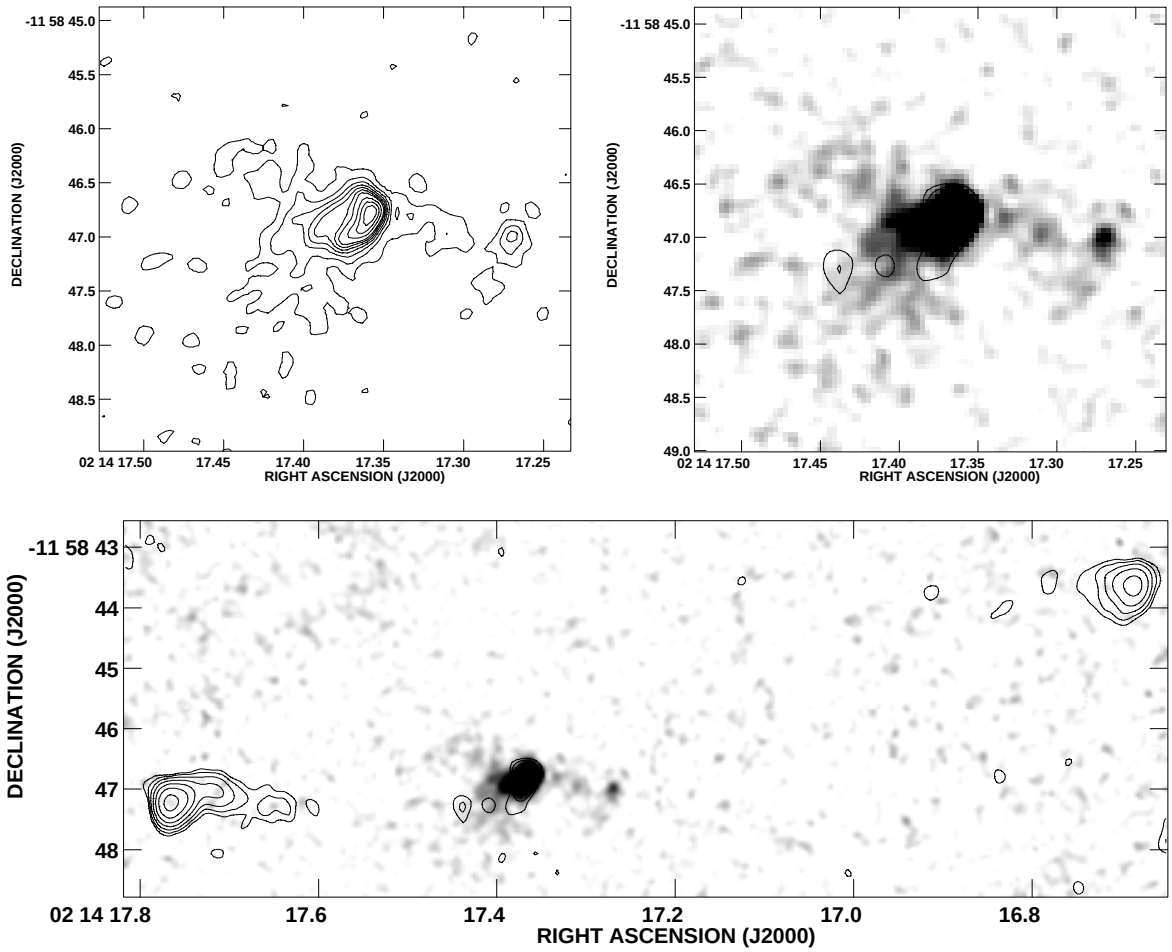

Fig. 8. *Top left*: Grey scale image of TX 0211-122 at z=2.336, with VLA radio contours superimposed. Contours are at a geometrical sequence in 2 with the first contour at 0.1 mJy. *Top right*: Contour representation of the UV continuum emission. Contour levels:8,9,10,12,14,16,18,20 $\times 10^{-21}$ erg s^{-1} Å^{-1}. *Bottom*: An image of the full field of the radio galaxy. Radio contours and grey scale are the same as the upper left panel.

this shear is almost equal to the overall velocity width of the line (van Ojik et al. 1997).

6. HZRGs morphologies and evolution

6.1. Radio optical alignment

The UV-optical continuum emission from HZRGs is generally aligned with the main axis of the radio emission; several models have been proposed to explain the nature of the optical continuum emission and of this alignment effect (for a review see McCarthy 1993 and references therein). The most viable ones are: (i) star-formation stimulated by the radio jets as it propagates outward from the nucleus (Chambers et al. 1987, McCarthy et al. 1987, de Young 1989, Daly 1990); (ii) scattering of light from an obscured nucleus by dust or free electrons (di Serego Alighieri et al. 1989; Scarrott et al. 1990; Tadhunter et al. 1992; Cimatti et al. 1993; di Serego Alighieri et al. 1994); (iii) nebular continuum emission from warm line emitting clouds excited by the obscured nucleus (Dickson et al. 1995).

So far the only HZRG for which there is direct spectroscopic evidence that the UV continuum clumps are star forming regions, not dominated by scattered light, is 4C41.17: the spectrum of this galaxy shows absorption lines and P-Cygni profiles similar to those found in the spectra of high redshift star forming galaxies (Dey et al. 1997).

Until recently, polarization measurements were possible only for z$\sim$ 1 radio galaxies and showed that in most cases a large fraction of the UV continuum emission could be explained as scattered light. Recently though, observations of $z \geq 2$ radio galaxies have led to quite contradictory results: while some objects show considerable amounts of polarization (e.g Cimatti et al. 1997 and references therein), others such as 4C41.17 have upper limits consistent with the complete absence of polarization (Dey et al. 1997).

The HST data with their high resolution provide informations about the inner regions of HZRGs, and confirm that the radio/optical alignment is still present at scales of less than an arcsecond. In Fig. 12 we plot the distribution of position angle difference ($\Delta\Theta$) for our sample. To determine the optical position angle (PA), for the galaxies with a more regular morphology we smoothed the HST images with a Gaussian function having a FWHM of 1″ and then we fit the inner 3″ region with ellipses,

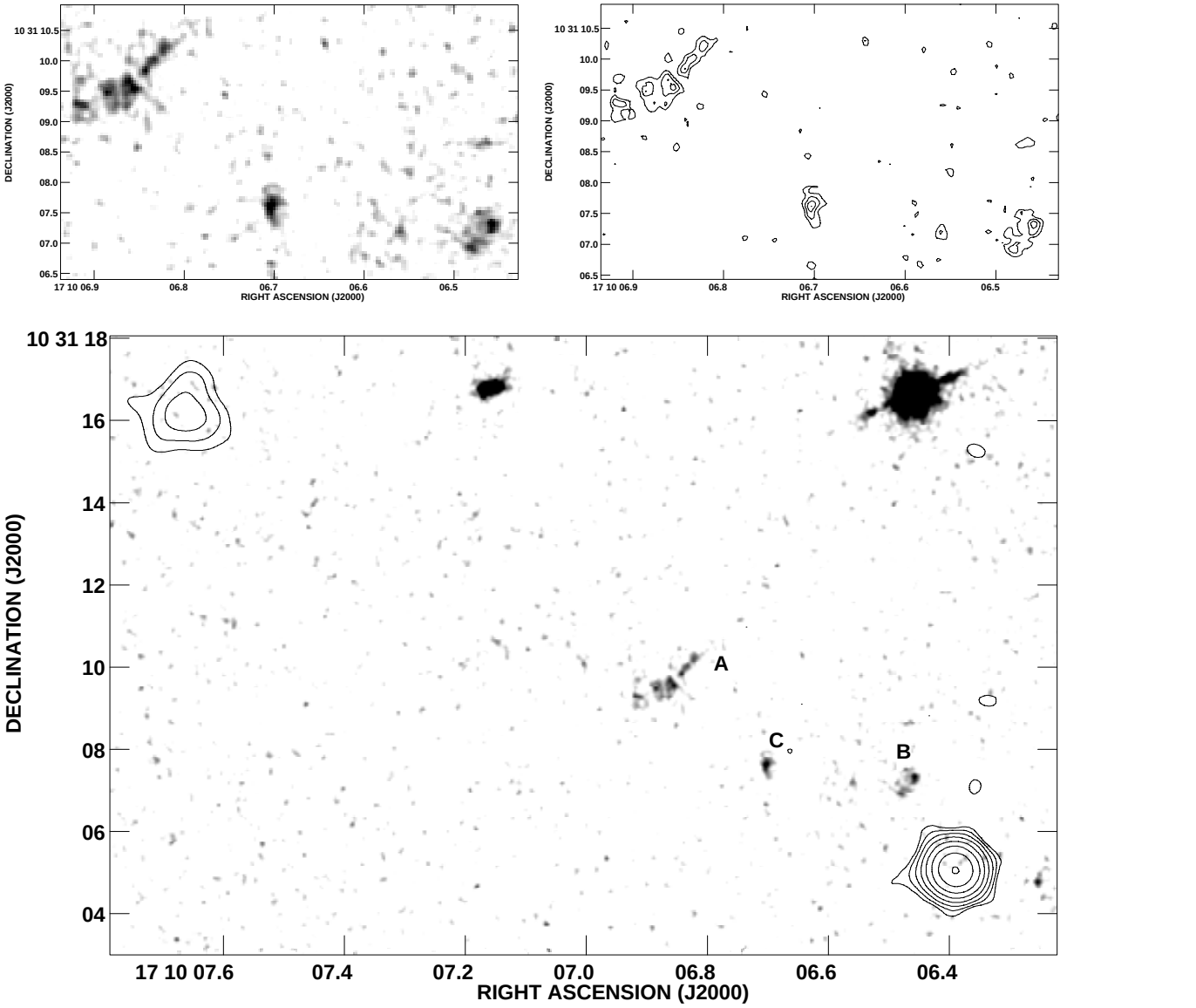

Fig. 9. *Top left*: Grey scale image of TX 1707+105 at z=2.349. *Top right*: Contour representation of the UV continuum emission. Contour levels: 10,11,12,13,14$\times 610^{-22}$ erg s^{-1} Å^{-1}. *Bottom*: Full image of the field of the radio source, with VLA radio contours superimposed. Contours are at a geometrical sequence in 2 with the first contour at 0.18 mJy.

using the IRAF package ISOPHOTE, which also gives the orientation of the major axis of the ellipse. For the galaxies with irregular morphologies, the fits gave meaningless results, so we selected as optical axis the line passing through the 2 brightest peaks on the images. The position angle of the radio emission is given by the line joining the radio core to the nearest hot spots (or the line joining the hotspots, if the core is not detected).

Despite the fact that 13 out of 15 radio galaxies in our sample have $\Delta\Theta \leq 45°$, we notice that the properties of the alignment effect vary considerably from object to objects.

We can distinguish various groups:

(i) Radio galaxies that show a remarkable one-to one relation between radio emission and UV continuum light: this includes 4C 1345+245, that has an optical jet-like feature, and 4C 1243+036 where the UV light follows the bending of the radio jet. These structures can be easily explained by the jet-induced star formation models (see references above). Alternatively Bremer et al. (1997) proposed a mechanism by which, when the radio jet passes through the gas clouds, it breaks them apart thus increasing the surface area of cool gas exposed to the ionizing beam. Consequently the material along the jet path becomes a far more efficient scatterer of nuclear radiation and the UV emission is enhanced in a very narrow region.

(ii) Radio galaxies in which the UV continuum emission has a triangular-shaped morphology, reminiscent of an ionization cone. This category includes TX 0828+193, MRC 2025−218 and MRC 0406-242. Such morphologies are expected in models that consider the aligned optical continuum as being scattered light of a central buried quasar.

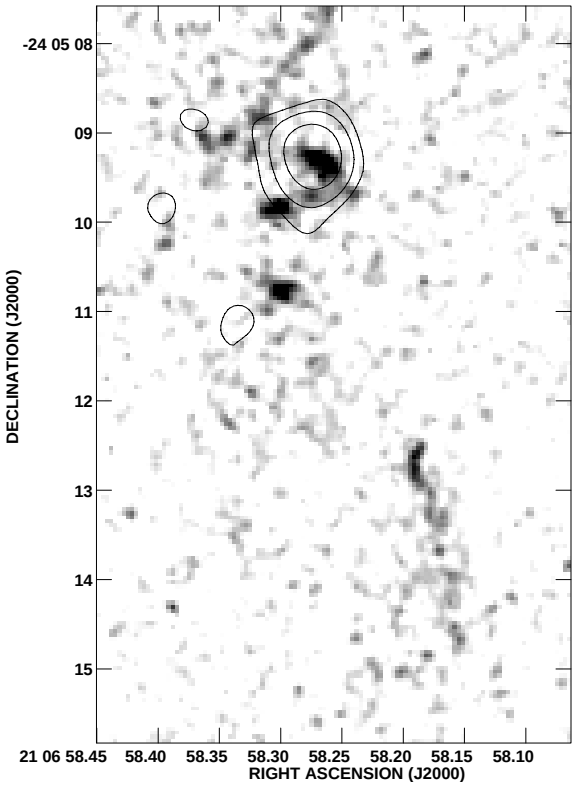

Fig. 10. Grey scale image of MRC 2104-242 at z=2.491, with VLA radio contours superimposed. Contours are at a geometrical sequence in 2 with the first contour at 0.07 mJy.

(iii) Radio galaxies where the alignment between the optical morphology and the radio axis is good but where there is no one-to one relation between radio and UV components. This group includes MRC 0943−242, MRC 2104−242, 4C 1410−001, TX 0211−122, MG 2141+192, PKS 1138−262, 4C28.58 and 4C41.17. The degree to which the two components are aligned varies strongly even within this group: for example in the radio galaxy 4C 1410-001 the difference in position angles between the radio and the UV emission is 45°, however the radio map indicates that the radio jets probably had a different direction in the past, corresponding to the direction along which the UV light is elongated.

(iv) Finally, galaxies that show total misalignment between radio and optical emission. There are 2 such cases in our sample. First the radio galaxy B2 0902+343 (Fig. 3), where dust could play an important role in obscuring the central regions (Eales et al. 1993, Eisenhardt & Dickinson 1992), thus "masking" the alignment effect. Second, the extremely peculiar and complex system TX 1707+105 (Fig. 9), which is comprised of 2 (possibly 3) separate galaxies, with similarly strong Lyα emission: the galaxies are located along the radio axis, but they are clumpy and extended almost perpendicularly to the radio axis. This unusual morphology would be hard to explain just by invoking the presence of dust, since the dust should have an extremely complicated distribution in multiple lanes parallel to the radio axis.

In summary the new data confirm that there is no single model that can satisfactorily explain the optical morphology of all HZRGs and the nature of the aligned optical continuum emission. At the same time, none of the proposed models can be ruled out by the present data. Therefore it seems likely that all three mechanisms contribute to the aligned light, but their relative importance varies greatly from object to object.

6.2. Clumpiness of the optical emission

A striking feature of the HST images of the radio galaxies is the widespread clumpiness of the optical continuum emission. Most galaxies are comprised of several components, regardless of the fact whether they are aligned or not with the radio axis; the clumps are resolved and their typical sizes are in the range 2-10 kpc. To give a consistent definition of "clumpiness" we proceeded in the following way: since the size of our sample is small, and for the faintest galaxies it is difficult to delineate the structures, we first normalized the total observed flux of each galaxy (within a fixed aperture) taking the faintest and most distant galaxy MG 2141+192 as reference. We then defined the parameter n as the number of components which have at least one contour at a flux level of $4.4\times10^{-19}(1+z)^{-4}$ erg cm^{-2} sec^{-1} Å^{-1}. This value was chosen so that the radio galaxy MG 2141+192 had 3 clumps. Note that, despite the difference in rest frame frequencies sampled by the observations (see Table 1), this is a good approximation because the spectral energy distribution of HZRGs in the UV wavelength range (1300-2000 Å) is generally flat.

In Fig. 13 we present a plot showing how n, our measure of clumpiness, varies with radio size, for all the radio galaxies in the sample. Clearly there is a tendency for the larger radio sources to have a clumpier optical continuum: the sources with radio sizes greater than ~ 80kpc have on average more than twice as many clumps as the smaller radio galaxies. A Spearman rank correlation test gives a significance level of 95% for this correlation.

A possible explanation for this trend is that the medium around the hosts of powerful AGN is dense and clumpy on a scale of more than 100 kpc; as the radio sources expand through the gas, they light up more and more material either by triggering star formation in the gas clouds, or by enhancing the scattering properties of the material in the vicinity of the jets. This result is contrary to that found by Best et al. (1996) for a complete sample of $z \simeq 1$ 3CR radio sources, which have been imaged with the HST: they found that smaller radio sources tend to be comprised of a string of several knots, while larger radio galaxies are made generally of only 2 optical components. However note that the range of radio sizes of the $z \simeq 1$ 3CR sample is 3 times as large as that of our sample.

6.3. Morphological evolution

Our sample covers a redshift range from z=2 to z=3.8, which corresponds to look-back times from 80% to 90% of the total age of the universe (for $\Omega = 1$). This epoch is close to the epoch

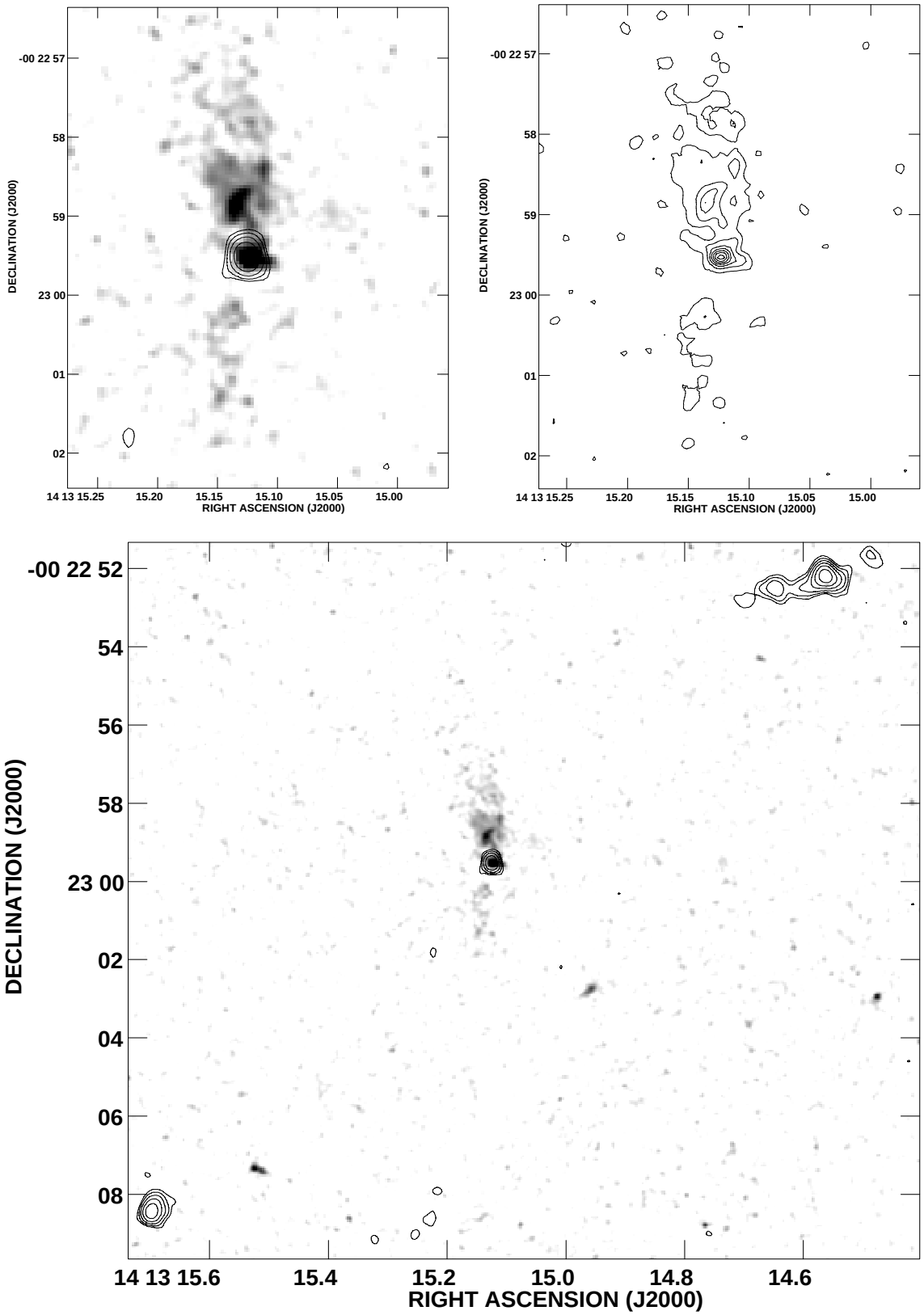

Fig. 11. *Top left*: Grey scale image of 4C 1410-001 at z=2.363, with VLA radio contours superimposed. Contours are at a geometrical sequence in 2 with the first contour at 0.11 mJy. *Top right*: Contour representation of the UV continuum emission. Contour levels:10,11,12,13,14,15,16 $\times 1.210^{-21}$ erg s^{-1} Å^{-1}. *Bottom*: An image of the full field of the radio galaxy. Radio contours and grey scale are the same as the upper left panel.

of the formation of these HZRGS, therefore it is interesting to search for any evolution in the properties of the radio galaxies with increasing cosmic time. We follow a similar approach to that used by van Breugel et al. (1998) for a sample of powerful HZRGs, observed with Keck in the near infrared, which corresponds to the restframe optical emission (> 4000 Å). Their sample is similar to ours, being comprised or a similar number of sources, with the same radio power, but has a higher average redshift ($z_{av} = 3.2$ versus $z_{av} = 2.8$) and more galaxies having $z \geq 3$. There are 6 radio galaxies common to both samples.

In Fig. 14 we present the results for our sample of HZRGs: the upper plot shows how the radio /optical size ratio varies with redshift; the radio sizes are measured as the distances between the most distant hot spots, on either side of the nucleus, while the optical lengths are defined to be the maximum extension of the optical emission in the direction of the radio source. In cases of multiple systems, such as PKS 1138-262 and TX 1707+105, all the optical components where considered, so that the radio/optical size ratio gives an indication of how much emission there is within the radio source extension. The plot indicates that there is no significant evolution in the ratio of radio to optical size. If we divide the sample in two redshift ranges, then the average radio/optical size ratio is 3.2 for the highest redshift bin ($z \geq 2.9$) and 3.4 for the lowest redshift radio galaxies, so the difference is negligible. This is different from the result of an Breugel et al. for the infrared emission: they present marginal evidence that the hosts of $z \geq 3$ radio galaxies are comparable in size with the radio sources, while the $z \leq 3$ radio sources appear systematically larger that the host galaxies.

In the bottom plot of Fig. 14 we show how the strength of the radio-optical alignment, represented by the difference in position angle between the optical and the radio emission $\Delta\Theta$ (see Sect. above for definition) varies with z. Again there is no significant difference between the lowest redshift radio galaxies, which have an average PA difference of $20^\circ \pm 7^\circ$[1] and the highest redshift sources which have an average of $18^\circ \pm 8^\circ$. On the contrary van Breugel et al. find a strong evolution in the alignment of the host galaxies from $z \geq 3$ to $z \leq 3$: specifically the infrared morphologies become smoother and less elongated at $z \leq 3$ and the infrared/radio alignment strength decreases. The best interpretation is that, while for the lower redshift sources in their sample the near IR emission is dominated by the most evolved stellar population, (which is less effected by the presence of the radio jets), for the very high redshift galaxies the observed near IR emission starts to be dominated by young stars, probably formed following the passage of the radio jets.

On the other hand, our HST observations sample the UV restframe emission which is thought to be dominated by the younger stellar populations in all cases, regardless of redshift. These young hot stars are formed in subsequent small bursts, induced either by the interaction of the jets with the medium

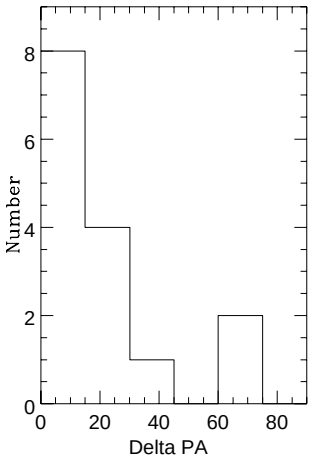

Fig. 12. Distribution of the differences in position angles between the radio emission and the UV continuum emission, measured in the inner 3″ region of the radio galaxies. The histogram includes data from the enlarged sample (see text).

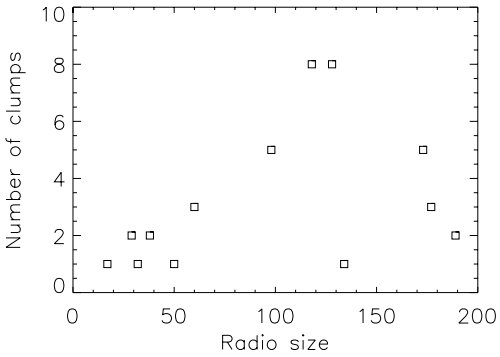

Fig. 13. Number of optical clumps of the galaxies versus total radio source size (in kpc).

or by mergers of smaller subunits. Such events may involve only little amounts of mass, but can still produce remarkable UV morphologies (e.g 1138-262 Pentericci et al. 1998), and their frequency is not expected to change from redshift 4 to 2. Therefore we don't expect any strong evolution in the UV restframe properties of the radio galaxies in this redshift interval.

6.4. The formation of brightest cluster galaxies?

It is interesting to compare the morphologies of our high-redshift radio galaxies with those of the high-redshift galaxies that have been discovered recently using UV dropout techniques and extensively studied (see for example Steidel et al. 1996, Giavalisco et al. 1996, Williams et al. 1996).

As pointed out in Sect. 6.1, a fraction of the UV continuum emission of HZRGs is directly connected, through various possible mechanisms, to the presence of the AGN. Also some of the features that we see in the galaxies can be easily explained by a direct correlation with the radio jets, for example the narrow elongated structures seen in 4C 1243+036 and MRC 2104−242 and the jet-like feature observed in 4C 1345+245. However in other cases there is a striking similarity between the *individ-*

[1] We preferred not to include the radio source TX 1707+105 in calculating the average PA of the low redshift group, because for this source the PA of the single galaxy 1707+105A, ($\sim 69^\circ$), is extremely different from the PA of whole system (3 galaxies, PA$\sim 13^\circ$)

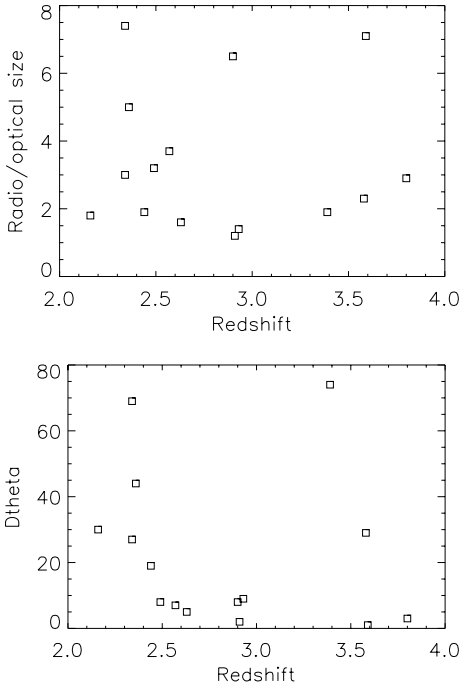

Fig. 14. Evolution of the alignment strength (*upper panel*) and the radio/optical size ratio (*lower panel*) with redshift.

ual components of the radio galaxies and the population of UV dropout galaxies, which clearly favors a stellar origin for the emission from those clumps.

Particularly in some of the clumpiest and most extended radio galaxies, such as TX 1707+105 and MRC 2104−242, there are components that have a compact and regular morphology, with sizes of the order of few kpc resembling that of the high redshift radio-quiet galaxies. In a previous paper we made a detailed comparison between the clumps associated with the radio galaxy 1138−262 and the UV dropout galaxies. Our conclusion was that those components had several characteristics similar to the UV dropout galaxies, e.g. absolute magnitudes, surface brightness profiles, half-light radii ($\sim$ 2 kpc) and inferred star formation rates (5-10 $M_{\odot}\mathrm{yr}^{-1}$ per clump; Pentericci et al. 1998). Also 4C41.17 has a similar very clumpy morphology with compelling evidence that the clumps are star forming regions. However, we note that since it is not yet possible to determine the masses of either UV dropouts or radio galaxy clumps, it may well be that they are intrinsically different objects, with a similar amount of star-bursting activity that makes them look similar in the UV continuum emission.

It seems that at least some of the high redshift radio galaxies consist of a central large galaxy, that hosts the AGN and a number of small star forming subunits, resembling the UV dropout galaxies, which are located in a region as large as $\sim 50-100$ kpc around the radio source. Powerful radio sources might then pinpoint regions in which the density of star forming units is higher than average. The central host galaxies of radio sources might have formed through merging of these small sub-galactic stellar systems. Note that the mergers of these gas-rich subunits with the host galaxies could have triggered (or re-triggered) the radio emission by providing fuel for the central engine of the AGNs, as it seen in many cases at low z (e.g Osterbrock 1993).

Our observations provide qualitative support for hierarchical galaxy evolution models, which predict that the morphological appearance of galaxies during their formation period should be highly irregular and clumpy (e.g Baron & White 1989). In particular semi-analytical models predict that one of the forms in which massive elliptical galaxies accrete their mass is from multiple merging of smaller subunits (Aragon-Salamanca et al. 1998, and references therein. A possible problem arises from the fact that in standard hierarchical cold dark matter models such massive systems are thought to form relatively late (Cole et al. 1994, Kauffmann et al. 1993), i.e. at much lower redshift, and in the majority of galaxies the main population of stars is formed more recently (after $z = 1$) Heyl et al. 1995. However, White & Frenk (1991) argue that a mechanism that could explain the formation of massive elliptical galaxies at an earlier epoch is over-merging of star-burst galaxies and indeed, as we have reviewed in the introduction, there is now increasing evidence that high redshift radio galaxies are probably located in the over-dense regions of the early universe.

Therefore we conclude that high redshift radio galaxies may be formed from aggregates of sub-galactic units, similar to the UV dropout galaxies, and will probably evolve into present–day brightest cluster galaxies.

7. Summary and concluding remarks

In this paper we have presented new HST/WFPC2 images of 11 high redshift radio galaxies, all complemented with VLA radio maps of comparable resolution. The images reveal a wide variety in galaxy morphology: in particular most of the objects have a clumpy, irregular appearance, consisting of a bright nucleus and a number of smaller components. The number of observed clumps increases with increasing radio size. The UV continuum emission is generally elongated and aligned with the axis of the radio sources, however the characteristics of the "alignment effect" differ greatly from case to case. The new data confirm that none of the proposed models can satisfactorily explain the phenomenon and that most probably the aligned continuum emission is a mixture of starlight, scattered radiation and nebular continuum emission. Our data show no significant evolution in the morphological properties over the observed redshift interval. Finally, we compare the properties of our radio galaxies with those of the UV dropout galaxies and conclude that high redshift radio galaxies might be forming from aggregates of sub-clumps similar to the UV dropout galaxies and that they will probably evolve into present day brightest cluster galaxies.

In a future paper we will present complementary HST/NICMOS data of an enlarged sample of high redshift radio galaxies. The new infrared observations will provide constrains to the age of the older stellar population of the host galaxies. With the high resolution we will be able to determine if also the older stellar population shows significant clumpy sub-structures and to what extent are the forming brightest cluster ellipticals already assembled and relaxed.

Table 3. Radio properties of TX 1707+105

Component	$S_{8.4}$ mJy	$S_{4.8}$ mJy	$I_{8.4}$ mJy/beam	$I_{4.8}$ mJy/beam	α	$S^p_{8.4}$ mJy	$S^p_{4.8}$ mJy	$FP_{8.4}$ %	$FP_{4.8}$ %	RM rad m^{-2}
NW	2.85	7.47	1.07	4.69	2.6					
SE	27.3	55.8	23.4	53.1	1.5	4.85	4.12	18	7.4	47

Table 4. Radio properties of MRC 2104-242

Component	$S_{8.2}$ mJy	$S_{4.8}$ mJy	$S_{1.5}$ mJy	$I_{8.2}$ mJy/beam	$I_{4.8}$ mJy/beam	$I_{1.5}$ mJy/beam	α_l	α_h
North lobe	22.9	55.2	294	10.4	49.8	278	1.45	2.9
Core	0.55			0.53				
South lobe	1.77	7.14	34.8	1.27	4.66	19.2	1.2	2.5

Acknowledgements. This work is based on observations with the NASA/ESA Hubble Space Telescope, obtained at the Space Telescope Science Institute, which is operated by AURA Inc. under contract with NASA. We thank C. Carilli for doing the reduction of the radio data for TX 1707+105. HJAR acknowledges support from an EU twinning project, a programme subsidy granted by the Netherlands Organization for Scientific Research (NWO) and a NATO research grant. The work by WvB at IGPP/LLNL was performed under the auspices of the US Department of Energy under contract W-7405-ENG-48.

Appendix A: radio images of TX 1707+105

We present here multi-frequency maps of the radio galaxy TX 1707+105 obtained with the VLA in B array.

Observations were made at 4.5 and 8.2 GHz, using two frequency channel each having a 50 MHz bandwidth, for a total integration time of 700 s and 1020 s respectively. Data processing was done performed using the Astronomical Image Processing System (AIPS) in the standard way. The system gains were calibrated with respect to the standard sources 3C286. Phase calibration was performed using the nearby calibrator 1658+076. The antenna polarization response terms were determined using multiple scans of the calibrator 1850+284 over a large range in parallactic angle. Absolute linear polarization position angles were measured using a scan of 3C286. The calibrated data were then edited and self-calibrated using standard procedures to improve the dynamic range. Images of the three Stokes polarization parameters, I, Q and U were synthesized and all images were CLEANed down to a level of approximately 3 times the theoretical rms noise using the AIPS task IMAGR. The observations at the different frequencies were added in the image plane to produce the the final maps of total and polarized flux.

In Fig. A1 we show the maps at 4.5 GHz and 8.2 GHz (with a resolution respectively of 1.2″ and 0.7″) of the total flux (left panels) and polarized flux (right panels). In all images contours are spaced in a geometric progression with a factor of 2, with the first contour level equal to 3σ, where σ the off-source rms which is 0.12 mJy for the 4.5 GHz map, 0.1 mJy for the 8.2 GHz map and 0.17 mJy for the polarized flux maps.

The radio galaxy has a simple double morphology with no radio core detected in the present images. The two lobes are nearly symmetric in total radio brightness, but the northern hot spot is totally depolarized at both frequencies, while the southern one is polarized.

Appendix B: radio images of MRC 2104-242

In Fig. B1 we present maps of the radio galaxy MRC 2104−242 obtained with the VLA in B array at 3 different frequencies: 1.4 GHz, 4.5 GHz, and 8.2 GHz, with a resolution, respectively of 3.9″, 1.2″ and 0.7″. In all images contours are spaced in a geometric progression with a factor of 2, with the first contour lever equal to 3σ, where σ the off-source rms, which is respectively at 1.74 mJy for the 1.5 GHz map, 0.19 mJy for the 4.5GHz map and 0.05 mJy for the 8.2 GHz map.

The radio source is a double showing fainter diffuse emission between the hot spots and the core. The northern hot spot is elongated in a direction the is different from the radio axis.

References

Aragon-Salamanca A., Braugh C.M., Kauffmann, G., 1998, MNRAS 297, 427
Armus L., Soifer B., Murphy T. W. Jr, et al., 1998, ApJ 495, 276
Baron E., White S. D. M., 1987, ApJ 322, 585
Best, P., 1996, in Bremer M., Carilli C., Röttgering H., van der Werf P. (eds.), "Cold Gas at High Redshifts", Kluwer
Best P., Longair M. S.,Röttgering H. J. A., 1997, MNRAS 286, 785
Bremer M. N., Fabian A. C., Crawford C. S., 1997, MNRAS 284, 213
Briggs, F. H., Sorar, E., and Taramopoulos, A., 1993, ApJ 415, L99
Burrows C., 1995, in Burrows C. (ed.), "Wide Field and Planetary Camera 2 Instrument Handbook", Baltimore: STScI
Carilli C., 1995, A&A 298, 77
Carilli C. L., Owen F. N., Harris D. E., 1994, AJ 107, 480
Carilli C. L., Rottgering H., van Ojik R., Miley G. K., van Breugel W., 1997, ApJS 109, 1
Carilli C. L., Harris D., Pentericci L., et al.,1998, ApJ 494L, 143
Chambers K. C., Miley G. K., van Breugel W.J.M., 1987, Nat 329, 604
Chambers K. C., Miley G., van Breugel W.J. M., et al., 1996a, ApJS 106, 247

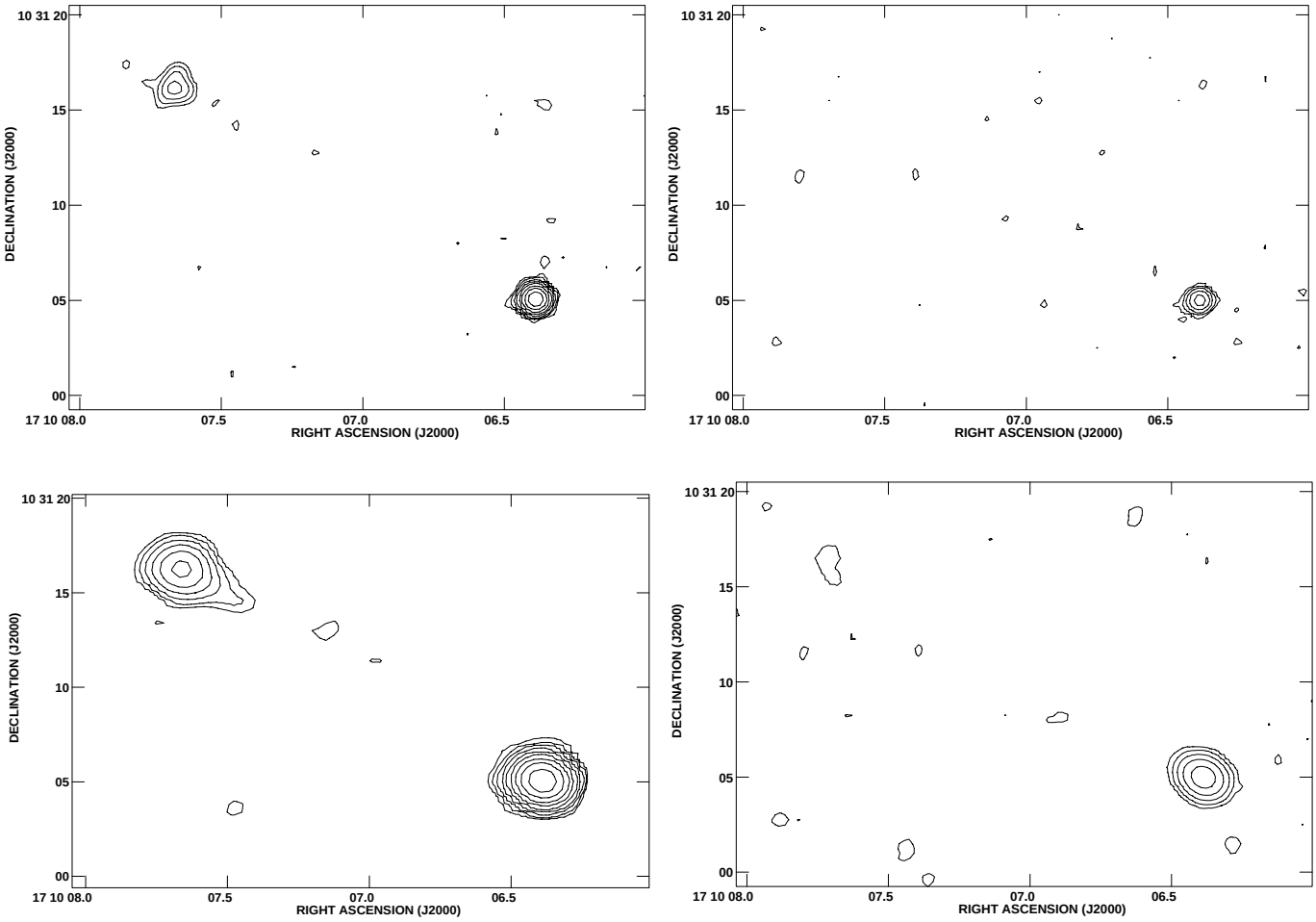
10 31 20
15
10
05
00
DECLINATION (J2000)
17 10 08.0
07.5
07.0
06.5
RIGHT ASCENSION (J2000)

Fig. A1.

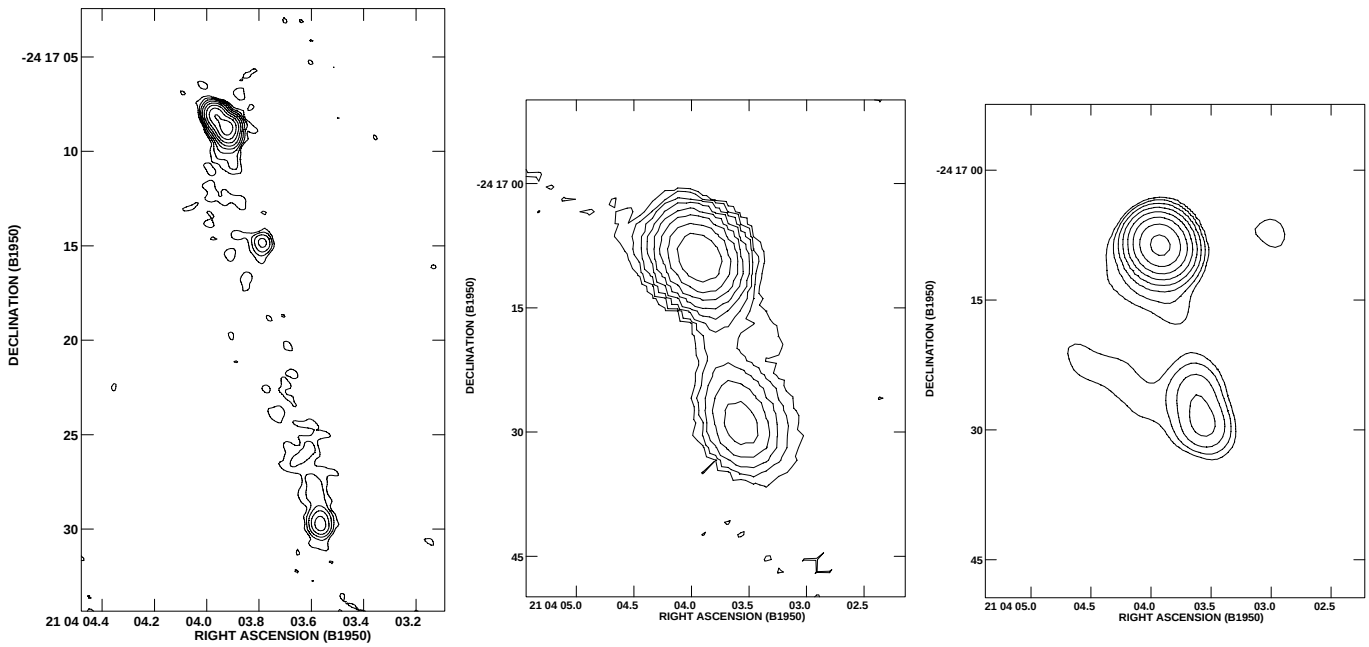
-24 17 05
10
15
20
25
30
DECLINATION (B1950)
21 04 04.4
04.2
04.0
03.8
03.6
03.4
03.2
RIGHT ASCENSION (B1950)
-24 17 00
15
30
45
21 04 05.0
04.5
04.0
03.5
03.0
02.5

Fig. B1.

Chambers K. C., Miley G., van Breugel W. J. M., Huang J. S., 1996b, ApJS 106, 215
Cimatti A., di Serego Alighieri S., Fosbury R., Salvati M. S., Taylor D., 1993, MNRAS 264, 421
Cimatti A., Dey A., van Breugel W., Hurt T., Antonucci R., 1997, ApJ 476, 677
Cole S., Aragon-Salamanca A., Frenk C. S., Navarro J. F., Zepf S. E., 1994, MNRAS 271, 781
Crawford C., Fabian A., 1996, MNRAS 282, 1483
Daly R. A., 1990, ApJ 355, 416
de Bruyn, G., 1996, in Bremer M., Carilli C., Röttgering H., van der Werf P. (eds.), "Cold Gas at High Redshifts", Kluwer
de Koff S. D., Baum S., Sparks W., et al., 1996, ApJ 621, 107
Dey A., van Breugel W., Vacca W., Antonucci R., 1997, ApJ 490, 698
de Young D. S., 1989, ApJ 342, L59
di Serego Alighieri S., Fosbury R. A. E., Tadhunter P. Q. C., 1989, Nat 341, 307
di Serego Alighieri S.,Cimatti A., Fosbury R. A. E., 1994, ApJ 431, 123
Dickinson M. et al., 1998 ApJ in press
Dickson R., Tadhunter C., Shaw M., Clarck N., Morganti R., 1995, MNRAS 273, L29
Eales S. A., Rawlings S., 1996, ApJ 460, 68
Eales S., Rawlings S., Puxley P., Rocca-Volmerange B., Kuntz K., 1993, Nat 363, 140
Eales S. A., Rawlings S., Law-Green D., Cotter G., Lacy M., 1997, MNRAS 291, 593
Eisenhardt P., Dickinson M., 1992, ApJ 47, 399
Giavalisco M., Steidel C., Macchetto F., 1996, ApJ 189, 470
HST Data Handbook, Version 2.0, December 1995, C. Leitherer ed.
Heyl J., Cole S., Frenk C., Navarro J., 1995, MNRAS 274, 755
Hill G., Lilly S., 1991, ApJ 367, 1
Holtzmann J., Burrows C., Casertano S., et al., 1995, PASP 107, 1065
Kauffmann G., White S., Guiderdoni B., 1993, MNRAS 264, 201
Koekemoer A., van Breugel W. J. M., McCarthy P., Bland-Hawthorn J., 1996, in Bremer M., Carilli C., Röttgering H., van der Werf P. (eds.), "Cold Gas at High Redshifts", p. 385, Kluwer
Lacy M., Rawlings S., 1996, MNRAS 280, 888
Lauer T., 1989, PASP 101, 445
Le Févre O. L., Deltorn J., Crampton D., Dickinson M., 1996, ApJ 471, L11
Lilly S., 1988, ApJ 333, 161
Martin-Mirones J. M., Martinez-Gonzales E., Gonzalez-Serrano J., Sanz J. L., 1995, ApJ 440, 191
Maxfield L., Spinrad H., Stern D., 1997, AAS 191, 104.09
McCarthy P. J., 1993, ARA&A 31, 639
McCarthy P., van Breugel W., Spinrad H., Djorgovski S., 1987, ApJ321, L29
McCarthy P., Spinrad H., van Breugel W. et al., 1990, ApJ 365, 487
McCarthy P. J., Persson S. E., West S. C., 1992, ApJ 386, 52
Meisenheimer K., Roser H. J., Hiltner P. R., et al., 1989, A&A 219, 63
Osterbrock, D.E.: "Astrophysics of gaseous nebulae and active galactic nuclei", University Science Books, 1989.
Pentericci L., Rottgering H., Miley G., Carilli C., McCarthy P., 1997, A&A 500, 580
Pentericci L., Röttgering H., Miley G.K., et al.,1998, ApJ 504, 139
Röttgering H., Miley G. K., 1996, in Walsh J., Danziger I. (eds.), "Science with the VLT"
Röttgering H., Hunstead R., Miley G. K., van Ojik R., Wieringa M. H., 1995, MNRAS 277, 389
Röttgering H. J. A., West M., Miley G., Chambers K., 1996, A&AS 307, 376
Rush B., McCarthy P.J, Athreya R.M., Persson S., 1997, ApJ 163, 484
Scarrott S. M., Rolph C. D., Tadhunter C. N., 1990, MNRAS 243, 5P
Spinrad H., Dickinson M., Schlegel D., Gonzalez R., 1992, AAS 181, 41.02
Steidel C. C., Giavalisco M., Pettini M., Dickinson M., Adelberger K. L., 1996, ApJ 462, 17
Tadhunter C. N., Scarrott S., Draper P., Rolph C., 1992, MNRAS 256, 53p
Uson J., Bagri D. S., Cornwell D. S., 1991, Phys. Rev. Letter 67, 3328
van Breugel W., Dey, A., 1993, ApJ 414, 563
van Breugel W., Filippenko A. V., Heckman T. M., Miley G., 1985, ApJ 293, 83
van Breugel W.J.M, Stanford S.A., Spinrad H., Stern D., Graham J.R., 1998, ApJ 502, 614
van Ojik R., 1995, Ph.D. thesis, University of Leiden
van Ojik R., Röttgering H., Miley G., et al., 1994, A&A 289, 54
van Ojik R., Röttgering H., Carilli C., et al., 1996, A&A 313, 25
van Ojik R., Röttgering H. J. A., Miley G. K., Hunstead R., 1997, A&A 317, 358
White S. D. M., Frenk C. S., 1991, ApJ 379, 52
Williams R., Blacker B., Dickinson M., et al., 1996, AJ 112, 1335